Mon. Not. R. Astron. Soc. **341,** 981–992 (2003)

The dwarf LSB galaxy population of the Virgo cluster – I. The faint-end slope of the luminosity function

S. Sabatini,[1⋆] J. Davies,[1] R. Scaramella,[2] R. Smith,[1] M. Baes,[1,3]† S. M. Linder,[1] S. Roberts[1] and V. Testa[2]

[1]*Department of Physics and Astronomy, Cardiff University, Queen's Building, PO Box 913, Cardiff CF24 3YB*
[2]*INAF-OAR, via di Frascati 33, 00040 Monte Porzio Catone, Roma, Italy*
[3]*Sterrenkundig Observatorium, Universiteit Gent, Krijgslaan 281-59, B-9000 Gent, Belgium*

Accepted 2003 January 31. Received 2003 January 29; in original form 2002 November 29

ABSTRACT

The widely varying dwarf galaxy counts in different environments provide a strong challenge to standard hierarchical clustering models. The luminosity function is not universal, but seems to be strongly dependent upon environment. In this paper we describe an automated procedure for detecting and measuring very low surface brightness (LSB) features in deep CCD data. We apply this procedure to large-area CCD survey fields of the Virgo cluster. We show that there are many more faint ($-10 \geqslant M_B \geqslant -14$) LSB galaxies than would be predicted from extrapolation of the Virgo cluster catalogue luminosity function. Over our limited range of measurement, the faint-end slope of the luminosity function becomes $\alpha = -1.6$. The luminosity function is flatter in the inner regions of the cluster than it is in the outer regions. Although these galaxies contribute a small fraction of the total stellar light of the cluster, they may contribute significantly to the mass in galaxies if they have large mass-to-light ratios similar to those recently measured for Local Group dwarf galaxies.

Key words: galaxies: clusters: individual: Virgo – galaxies: dwarf – galaxies: fundamental parameters – galaxies: luminosity function, mass function.

1 INTRODUCTION

The Virgo cluster offers the best opportunity to study in detail large numbers of galaxies (also dwarf galaxies) over a small region of sky. It is the nearest ($d \sim 17$ Mpc, Tikhonov, Galazutdinova & Drozdovskii 2000) cluster with several hundreds of galaxies (∼1277 members, Binggeli, Sandage & Tarenghi 1984) and the largest dominant structure of the Local Supercluster. It is an irregularly shaped cluster, with a high abundance of spiral galaxies among the bright cluster members and a large population (80 per cent of the total known galaxy number) of dwarf galaxies (Binggeli et al. 1985). Its size is approximately 10° across the sky, which corresponds to ∼3 Mpc. The crossing time for this cluster is $\approx 0.1\ H^{-1}{}_0$ (Trentham & Tully 2002) so that cluster galaxies have had plenty of opportunities to interact with each other. The huge mass of the cluster ($M = 1.2 \times 10^{15}\ \mathrm{M}_\odot$, Fouque et al. 2001) accelerates the member galaxies to very high peculiar velocities, so that it exhibits the highest blueshift measured for any galaxy (IC3258, approaching us at 1600 km s^{-1}). As suggested from its irregular structure, the cluster is made up of at least three subclusters dominated by the bright ellipticals M87, M86 and M49 and thus it is probably not in a state of equilibrium; it is a very complex unrelaxed system where the central part is dynamically old, while the large surrounding region is not virialized, but still infalling (Bohringer 1995).

The first observations of the cluster date back to Mechain and Messier (late 18th century), who noticed a large concentration of nebulae in the northern wing of the Virgo constellation. The identification of the cluster as a self-gravitating system consisting of hundreds of galaxies followed soon after Hubble's 1923 discovery of Cepheids in M31. The first systematic investigation of the cluster was carried out by Shapley & Ames (1932). Since then the Virgo cluster has been of primary importance for extragalactic astronomy. It has been subject to many studies at optical, radio, infrared (IR) and X-ray wavelengths aimed at addressing its galaxy population, evolution and gas content; for the most recent studies, see Gavazzi et al. (2002) (optical and multiλ), Van Driel et al. (2000) (radio), Tuffs et al. (2002) (IR), and Shibata et al. (2001) (X-ray).

The most complete optical survey of the Virgo cluster was carried out by Binggeli et al. (1984), using photographic plates and a visual detection method. Whilst the advantage of using photographic plates is the wide area of sky surveyed (≈6° around the centre of the cluster in this case), the major disadvantage is the low sensitivity: the survey is incomplete for objects with $M_B \leqslant -14$, missing the numerous

⋆E-mail: s.sabatini@astro.cf.ac.uk
†Postodoctoral Fellow of the Fund for Scientific Research, Flanders Belgium (FWO-Vlaanderen).

galaxies that dominate the numbers in the Local Group, for example. Binggeli et al. (1984) carried out an extensive systematic study of the cluster finally producing a catalogue of 2096 galaxies, the Virgo Cluster Catalogue (VCC). The papers produced by them contain photometry and morphology for the galaxies, analyse morphology and dynamics and study specific and general luminosity functions (LFs) for the cluster (Binggeli et al. 1984, 1985, 1987; Sandage & Binggeli 1984; Sandage, Binggeli & Tammann 1985a,b).

Our main concern in this paper is with the numbers of faint Virgo dwarf galaxies that the subjective, visual detection method used by Binggeli et al. and others might have missed in less deep surveys. The observed galaxy counts are quantified by a determination of the galaxy LF (described by a Schechter function) and particularly from the value of its faint-end slope, α. After correction for incompleteness, Binggeli et al. found a value for the faint-end slope of $\alpha \sim -1.35$. Following on from the survey of Binggeli et al., Impey, Bothun & Malin (1988) used a photographic amplification technique to reach lower surface brightnesses. They found numerous additional LSB dwarf galaxies not included in the VCC and derived a value of $\alpha \sim -1.7$. Using the same technique, they also obtained a steepening in the faint-end slope of the Fornax cluster from -1.3 to -1.55 (Bothun et al. 1991).

A more recent study of the Virgo cluster by Phillipps et al. (1998a) (again using photographic plates) produced a steeper slope again ($\alpha \sim -2.0$). Phillipps et al. used a statistical method to obtain the LF, subtracting the faint galaxy number counts of fields outside the cluster from those containing the cluster. This technique is very delicate because two large numbers are being subtracted from each other to leave a small residual. There are also large variations in the background counts (Valotto, Moore & Lambas 2001). These rather steep values for the faint-end slope of the LF of Virgo are consistent with some values obtained for other clusters. For example, Bernstein et al. (1995) found a value of $\alpha \sim -1.4$ for the more distant Coma cluster while Kambas et al. (2000) found a very steep slope of $\alpha \sim -2.0$ for the nearby Fornax cluster.

These values differ, however, from recently determined values of the faint-end slope of the field galaxy population derived from the extensive two degree field (2dF) and Sloan surveys, where $\alpha \sim -1.2$ (Cross et al. 2001; Blanton et al. 2001). The field galaxy LF also corresponds very well with that obtained for the Local Group, $\alpha \sim -1.1$ (Mateo 1998).

A major concern with the measurement of the dwarf galaxy content in different environments is the wide range of data and detection methods used by different groups and how this affects the derived value of the faint-end slope. We have recently looked at fields in different environments (Sabatini, Roberts & Davies 2002; Roberts et al. in preparation) using data in exactly the same conditions as described below for Virgo. Trentham & Tully (2002) found that the LF is strongly dependent upon environment and, as a preliminary result, we find very few dwarf galaxies in the field and around isolated galaxies, if compared with numbers in Virgo.

It is clear that an environmental dependency of the LF places new and challenging constraints on current theories of galaxy formation. For example, standard cold dark matter (CDM) theories predict steep faint-end slopes in all environments (Bullock, Kravtsov & Weinberg 2000). Additions to the theory, such as supernovae driven winds (Dekel & Silk 1986) or the influence of a reheated intergalactic medium (Efstathiou 1992) have been used to suppress dwarf galaxy formation globally. These arguments cannot be used to explain the large differences in the dwarf galaxy population content in some environments. Recently, Tully et al. (2002) have suggested that dwarf galaxy numbers in different environments depend on whether the structure in which they reside is formed before or after reionization ('squelching'). They compared the Virgo cluster, which is dwarf-rich, to the dwarf-poor Ursa Major cluster. From their simulations they suggest that Virgo was assembled with its dwarf galaxy population before reionization and Ursa Major after, so that dwarf galaxy formation was suppressed. There is though, as they say, only 'qualitative' agreement between the model and the observations. Moore et al. (1999) offer more of a nurture rather than a nature explanation to the problem. Their galaxy 'harassment' model provides a mechanism for the formation of dwarf galaxies in the cluster environment through disruption of discs due to tidal interactions with the cluster and individual galaxies. The nature of the dwarf galaxy population is then very dependent on the dynamical properties of the cluster (crossing time, galaxy number density). The Virgo cluster has a very short crossing time ($0.1\ H^{-1}{}_0$) compared to Ursa Major ($0.5\ H^{-1}{}_0$) (Tully et al. 2002). Thus, the Virgo cluster galaxies have had more opportunities to become 'harassed'. In a study of the dynamical properties of Virgo cluster galaxies Conselice, Gallagher & Wyse (2001) describe evidence supporting the idea that the dwarf galaxies are dynamically distinct from the older cluster galaxy population and have thus been derived from an infalling population as envisaged by the harassment model of Moore et al. (1999).

An accurate derivation of the dwarf galaxy population as a function of environment is the only way to distinguish between these models. We need a detailed comparison of the LF derived consistently for galaxies in different environments with those predicted by CDM, squelching and harassment. This is the first of a series of papers in which we will study in more detail the dwarf galaxy population identified in Virgo and then we will derive the environmentally-dependent LF of galaxies for comparison with the models.

Dwarf galaxies are extremely difficult to detect because they generally have both very low luminosity and surface brightness. To detect objects like this we need an optimum filter to enhance the signal and a set of selection criteria that preferentially selects cluster members rather than background galaxies. We also require an automated and repeatable procedure that can be applied consistently to data taken from a large area survey.

The paper is organized as follows. In Section 2 we present the Isaac Newton Telescope (INT) Wide Field Camera (WFC) survey data (http://www.ast.cam.ac.uk/~wfcsur/index.php). In Section 3 we discuss the methods used to determine cluster membership and to assess possible background contamination. In Section 4 we describe the detection algorithm (see also Sabatini et al. 1999; Scaramella et al., in preparation). The LF and first results are presented in Section 5.

2 DATA

The data we use are part of the INT WFC survey, which is a multicolour CCD-based wide-field survey covering an area of $\sim$200 deg^2. The camera is mounted at the prime focus of the 2.5-m INT on La Palma, Canary Island, it consists of four thinned EEV 2 $\times$ 4 k^2 CCDs with pixel size of 0.33 arcsec and it has a field size of 34.2 $\times$ 34.2 arcmin^2 (neglecting the 1-arcmin interchip spacing). The data for the Virgo survey were acquired during observing runs in Spring 1999 to 2002 and consist of two perpendicular strips of *B*-band and *I*-band CCD images extending from the centre of the cluster (identified as M87) outward for 7° and 5°, respectively (see Fig. 1). The total area covered is $\sim$25 deg^2 and the average sky noise corresponds to $\sim 26B$ mag arcsec^{-2}. With the use of the techniques we describe in Section 4, these deep data allow us to study the

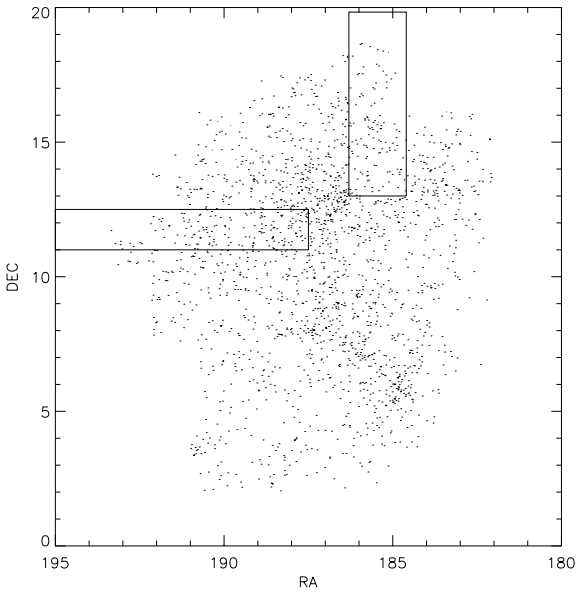

Figure 1. Plot of the Virgo cluster members as from the VCC. Overlayed are the areas covered by the INT WFCS.

population of dwarf galaxies down to very faint limiting central surface brightnesses ($\sim$26 B mag arcsec^{-2}) and absolute magnitudes ($M_B \sim -10$) (see below). The results presented in this paper make use of the east–west strip, that includes M87.

The data were preprocessed and fully reduced using the Wide Field Survey pipeline. This includes de-biasing, bad pixel replacement, non-linearity correction, flat-fielding, defringing (for I- and Z-bands) and gain correction. The photometric calibration makes use of several (5–10 per night) standard stars and the zero-points are accurate to 1–2 per cent. For details, see http://www.ast.cam.ac.uk/$\sim$wfcsur/pipeline.html. World Coordinate System (WCS) information is embedded in the reduced images FITS header and the astrometric calibration errors are $\leqslant$1 arcsec. The median seeing was 1.9 arcsec.

3 MEMBERSHIP DETERMINATION AND BACKGROUND SUBTRACTION

Membership determination is one of the crucial and controversial problems in the study of galaxy populations in nearby clusters (Valotto et al. 2001). The properties of the background galaxies need to be studied in detail in order to minimize contamination in the sample. With the aim of deriving selection criteria which will enable us to separate cluster from background galaxies, we have carried out numerical simulations of the galaxy population in order to identify distinguishing properties of member and non-member galaxies. The final goal is to find selection criteria that minimize the background contamination in the sample and at the same time maximize the number of Virgo cluster members selected. We have then tested the validity of the derived selection criteria in two ways (see ahead):

(i) by considering the fall in surface density of our detections with increasing distance from the cluster centre;

(ii) by measuring the number of background galaxies detected, using our selection criteria, on fields outside the cluster.

3.1 Numerical simulations of a cone of the universe

The effects of redshift on the apparent properties of a galaxy are mainly the following:

(i) surface brightness dimming due to distance (with a dependency of $(1 + z)^4$ + K-corrections);
(ii) change in apparent size with distance.

As a result, in principle, an intrinsically bright distant galaxy may appear as a faint nearby LSB galaxy and could be included in the cluster members catalogue. For example an L_* galaxy ($M_B = -20$, $\mu_0 = 21.7$ B mag arcsec^{-2}) at $z = 0.2$ has an apparent total magnitude of 19.5 and μ_0 of 23 and could be mistaken for a cluster low luminosity LSB galaxy. Its scale size however would be small (of the order of 2 arcsec) while a cluster dwarf with the same apparent magnitude would have a surface brightness of 24.3 B mag arcsec^{-2} (because of the surface brightness magnitude relation, see below) and hence a scale size of the order of 4 arcsec. Thus, in principle, cluster galaxies can be distinguished by their larger sizes and fainter surface brightnesses at a given magnitude.

In order to quantify the trend of the apparent parameters of a galaxy with redshift we have carried out some numerical simulations. We adapted a code (Morshidi-Esslinger 1997) that populates a cone of the universe and detects the galaxies after applying given selection criteria. The aim is to obtain an estimate of the completeness and contamination[1] of our sample for different selection criteria. We then use the most efficient selection criteria that preferentially select Virgo cluster galaxies. The code is composed of two parts:

(1) input galaxy creation;
(2) detection of the galaxies.

The cone of the universe is randomly uniformly[2] populated in space using a given cosmology, a LF and a surface brightness distribution for the galaxies. The output of this first part of the code is a catalogue of objects with given proper distance, apparent magnitude, central surface brightness and scalelength (all objects are assumed to have exponential profiles). In the second part of the code, the given selection criteria are applied to the catalogue and the final output is a list of the objects that satisfy the selection criteria along with their photometric properties.

In our simulations we chose $H_0 = 75$ km s^{-1} Mpc^{-1}, a flat universe with $\Omega_M = 0.3$ and $\Omega_\Lambda = 0.7$ (Lahav et al. 2002), and we analysed a cone from redshift 0.001 to 1.5 and size 10×10 deg^2.[3]

The LF we adopted for the field is that obtained by the 2dF Galaxy Redshift Survey (Madgwick et al. 2002) with the following parameters:

- $M_B* = -19.79$;
- $\alpha = -1.19$;
- $\phi_* = 0.00157$ h^3 Mpc^{-3}.

[1] In what follows by completeness we mean the ratio of the number of Virgo members selected according to the selection criteria to total Virgo members in the simulation. In the same way, the contamination is given by the ratio of the number of background galaxies selected to total number of galaxies (Virgo members + background).

[2] Density fluctuations are not considered here, as the main goal of the simulation is to compare general apparent properties (morphology and photometry) of the background population with the Virgo cluster galaxies.

[3] The large aperture is necessary because otherwise the local universe is under-represented, due to the very small volume. Moreover, this is also roughly the size of the cluster.

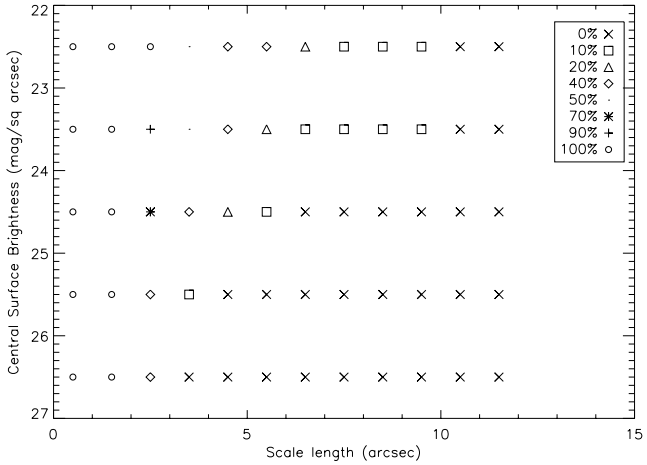

Figure 2. Plot of background contamination as a function of μ_0 (mag arcsec^{-2}) and h (arcsec). The numbers refer to the simulation where the LF has a faint-end slope of -1.4 for the Virgo cluster.

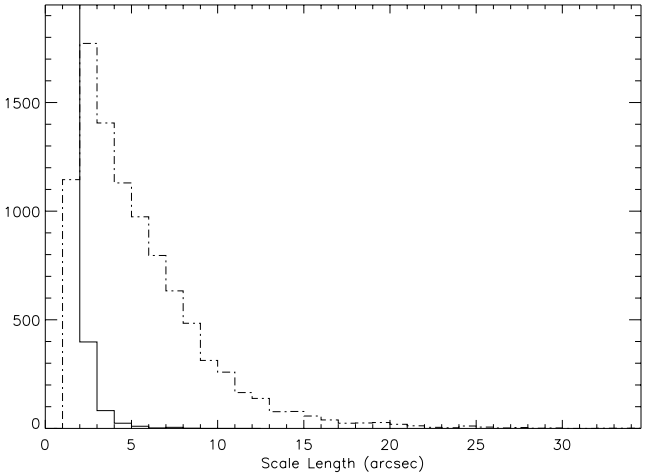

Figure 3. Histogram of scalelength for both simulations. The dashed-dotted line refers to Virgo members and the solid line to background galaxies.

The range of input magnitudes for the galaxies is -23 to -10.

The surface brightness distribution was chosen to follow the relationship between surface brightness and total magnitude (for recent confirmation see Blanton et al. 2001). Here we use that given in Driver (1999)

$$\mu_e \sim [(0.67 \pm 0.08)M_B - (33 \pm 6)] \quad (1)$$

where μ_e is the average surface brightness within the effective radius and for an exponential profile

$$\mu_e \sim \mu_0 + 1.15. \quad (2)$$

Using the same code with the same area – but keeping a fixed redshift of $z = 0.0040 \pm 0.0003$, corresponding to the distance of the Virgo cluster (Russell et al. 2000) – we generate an artificial cluster. The LF used to describe it is normalized to that in Sandage et al. (1985) in their survey of the Virgo cluster:

- $M_* = -21.4$ B mag;
- $\phi_* = 2.36$ Mpc^{-3}.

We leave the slope α as a free parameter, with the purpose of running simulations with different values ($\alpha = -1.0, -1.2, -1.4, -1.6, -1.8, -2.0$). The surface brightness distribution chosen to describe the Virgo cluster is the surface brightness magnitude relationship as derived by Impey et al. (1988) for Virgo:

$$\mu_0 = 0.67M + 32 \pm 2. \quad (3)$$

The output catalogues produced by the code allow us to study the behaviour of apparent central surface brightness, scalelength and total magnitude for simulations of the two different environments. We can then estimate what is the percentage of Virgo members and background galaxies for each bin of scalelength h and central surface brightness μ_0. In Fig. 2 we show how the percentage contamination by background galaxies depends on the scalelength and central surface brightness of the galaxy, for the simulation with $\alpha = -1.4$ for the Virgo LF.[4] Fig. 3 shows the histogram of scalelengths for all simulated galaxies. The dashed-dotted line refers to cluster members and the filled line to background galaxies. Both figures clearly show that the best discriminating property to distinguish cluster galaxies from background ones is the scalelength. As a general trend the background galaxies appear to have mainly smaller sizes and this makes it possible to separate them from Virgo members (as discussed earlier). Selecting galaxies with scalelengths $h \geqslant 3$ arcsec ensures that we maximize the detection of cluster galaxies compared to background galaxies (from Fig. 2, contamination within this selection criteria is kept under 50 per cent). Being primarily interested in the LSB population of the cluster we then restrict the selection to galaxies with $\mu_0 \geqslant 23$.

Simulations with LF faint-end slopes for the cluster steeper than that of the background give a better discrimination between cluster and background galaxies as the cluster slope increases. This is illustrated in Tables 1, 2 and 3.

In summary, our simulations have shown that in order to maximize the ratio of Virgo members to background galaxies we should use a selection criteria of $\mu_0 \geqslant 23$ and a scalelength $h \geqslant 3$ arcsec. On a practical note, we found that typically the seeing on our frames was a poor 2 arcsec. Convolving a 3-arcsec scale size galaxy with this seeing leads to a measured scale size closer to 4 arcsec. Thus, in practice we selected objects with measured scale sizes greater than

Table 1. Completeness and contaminations for different choices of the minimum scalelength selected.

Scalelength cut-off	Completeness (%)	Contamination (%)
Slope of Virgo LF $= -1.0$		
2	93	62
3	83	31
4	72	15

Table 2. Completeness and contaminations for different choices of the minimum scalelength selected.

Scalelength cut-off	Completeness (%)	Contamination (%)
Slope of Virgo LF $= -1.4$		
2	88	6.0
3	70	2.0
4	55	0.8

[4] We show results from this simulation because this is the flattest LF faint-end slope we would expect if we do not find any additional galaxy to the VCC ones.

Table 3. Completeness and contaminations for different choices of the minimum scalelength selected.

Scalelength cut-off	Completeness (%)	Contamination (%)
Slope of Virgo LF $= -2.0$		
2	82	0.02
3	60	0.00
4	44	0.00

3 arcsec which, because of the template sizes used in the method described below, means a minimum scale size of 4 arcsec.

3.2 Offset fields

As a further check to validate our selection criteria, we have applied our algorithm (see Section 4) to another set of INT WFC data using the same detector, exposure time and filter and covering a region of sky at about the same Galactic latitude. The data we have used are part of the Millennium Galaxy Survey, which is a 36-arcmin wide strip going from J2000 $9^h58^m28^s$ to $14^h46^m45^s$ (Liske et al. 2003). From these data we chose a number of random fields to compare our predicted number of background detections with that of the model. The number of galaxies detected by our algorithm is four galaxies per deg^2. This number is in agreement both with what our numerical simulations predicted ($\sim$ six galaxies per deg^2) and from what we measure for the background counts to be in the Virgo fields. It is much less than the actual number of galaxies ($\approx$20 galaxies per deg^2) found in the Virgo cluster fields. All these points are discussed further below.

4 THE DETECTION ALGORITHM

Looking for objects with a surface flux close to the sky noise requires the use of image enhancement techniques in order to optimize their detection. Standard detection algorithms for connected pixels in fact often fail on these types of objects because of their poor pixel-to-pixel signal-to-noise ratio (S/N). The algorithm we have developed uses frequency domain techniques and mainly consists of convolutions of the image with matched filters. The advantage in this case is the use of the total flux of the galaxy to detect it, instead of the very low S/N pixels at its edge. As an example of this, in Fig. 4 we show the finding chart produced by SExtractor (Bertin & Arnouts 1996) for one of our fields: a LSB galaxy from our catalogue ($\mu_0 =$ 25.3 mag arcsec^{-2}, $h = 9$ arcsec) is at the centre of the image. As a comparison we also show the output of our detection algorithm on the same image; where SExtractor finds many distinct objects at the position of the LSB galaxies, our procedure clearly distinguishes it as one.

The algorithm we have used is a modified version of the method described in Sabatini et al. (1999)[5] (for more details see Scaramella et al., in preparation) and it is composed of the following steps:

(i) background fluctuation flattening;

(ii) removal of standard astronomical objects (such as stars, bright galaxies, cosmic rays etc.);

(iii) image convolution with matched filters that are optimized to enhance faint fuzzy structures;

(iv) candidate classification.

[5] Data management and processing is performed using the application package language IDL (Copyright Research System, Inc.).

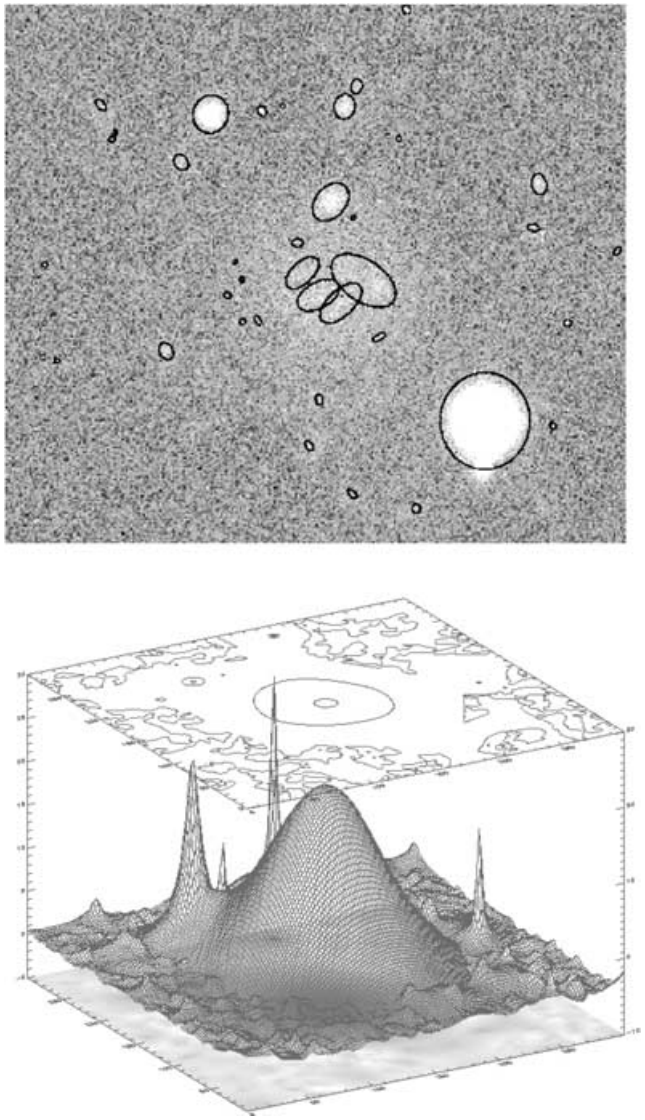

Figure 4. At the top we show the output of SExtractor for an image with a LSB galaxy from our catalogue in the centre. As can be seen, the program classified galaxy is identified as a group of small objects rather than as an object as a whole. The detection in this case is difficult because of the poor pixel-to-pixel S/N for this object. For comparison, at the bottom we show the three-dimensional output image from our algorithm for the same field. In this image the galaxy appears to be far above the noise level and thus easily detectable as a single object.

LSB and dwarf galaxy candidate identification is performed on the final convolved image by means of selecting all peaks that are significantly (see Section 4.3) above the residual noise fluctuations. The whole procedure (that includes masking, filtering, detection and measurement) is automated and its efficiency has been tested using artificial galaxies added to real images (see Section 4.5).

Techniques involving convolution with matched filters have been used before (see, for example, Armandroff, Davies & Jacoby 1998 or Flint et al. 2001) but the innovations of our method are mainly:

(1) a generalization of the use of the convolution – we make use of a set of filters with several different sizes and we then combine all the convolved images in just one final significance image where

objects of different scalelengths are emphasized at the same time (see Section 4.3);

(2) an optimization of the detection and photometry operations, that are performed at the same step using the final significance image (see Sections 4.4 and 4.5 for more details).

4.1 Preliminary processing

A very important issue when optimizing the detection of LSB galaxies is ensuring that the sky is as flat as possible across the image. Although the INT WFCS pipeline provides flat-fielded images, we use an automatic tool from the package SExtractor in order to remove possible residual background fluctuations. The technique consists of creating a map of the background sky by interpolation of the mean values of pixels in a grid of the original image. The grid size is chosen so as to preserve the biggest scalelength we want to detect with our convolution technique. Noise reduction gained in this way is about 6 per cent, but a flatter background allows an easier and less contaminated application of filters and a subsequent improved measure of source fluxes.

4.2 Removal of stars and standard objects

Before convolving the image with the set of filters, we remove all the 'standard' astronomical objects, such as stars, very bright galaxies, satellite tracks, hot pixels, etc. This is necessary in order to minimize the contamination of the sample by spurious objects, i.e. objects that could simulate LSB galaxies when convolved with the filters.

The masking procedure is performed in two steps in which different types of objects are considered. The first step is aimed at the removal of big and bright objects, such as saturated stars or bright galaxies, and the second step is aimed at small stars. Although SExtractor has the option of giving a cleaned output image, the removal is not always effective and many stellar haloes remain. We have thus written our own code for bright or saturated objects and we use the SExtractor procedure for the few small stars left over after our cleaning. Removal is performed by masking these objects with the local median sky value with added Poissonian noise. We use SExtractor just to detect all the standard objects in the image and select those to reject using a criterium based on dimension (isophotal area) and peak flux (surface isophotal flux weighted by peak flux), which clearly discriminates a stellar locus, a possible region of saturation and a region occupied by diffuse objects such as galaxies (Fig. 5).

Once the different regions in the plot are recognized, it is possible to identify the objects we want to mask (Fig. 5).[6] The stellar locus is fitted on each image so that the procedure is not affected by any change in the seeing value. Once the stellar locus is fitted we consider a line with the same slope but a constant coefficient lower of $1.5\sigma_{\rm fit}$, and we mask all the objects that are above this line. The object removal is performed masking the region with the median sky value plus its Poissonian noise. The size of the mask depends on the geometrical parameters that SExtractor gives for each object (elliptical axis and Kron radius), on peak intensity and on the radius at which the star flux falls below $1\sigma_{\rm sky}$.

Finally the removal of small stars left after this procedure is carried out using the star-subtracted image given by SExtractor. We obtain, in this way, a 'star-cleaned' image.

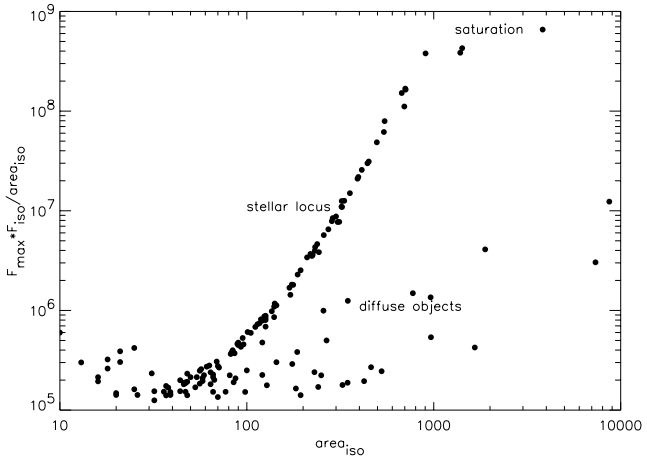

Figure 5. SExtractor detections for one of our typical images shown in the plane (isophotal area, surface isophotal flux weighted by peak flux). It is clearly possible to discriminate the stellar locus, a region of saturation and a region occupied by diffuse objects such as galaxies.

The star-masking procedure decreases the useful area for galaxy detection, so we take this into account when calculating numbers per deg^2 in the cluster.

4.3 The multiscale filter

The first problem when choosing the best filter for the detection of LSB or dwarf galaxies is the determination of the optimal scale size for the filter – the sizes of these galaxies are highly variable. The necessity of selecting many different scales requires the use of either a very wide bandpass filter (with the unavoidable consequence of including many different kind of objects) or the application of many different filters where we analyse the result from each one of these, requiring a huge working time. Thus we decided to build a procedure in which we apply a combination of filters of different sizes but we obtain (as described below) just one final significance image. This final image has the property of having each different size emphasized in it at the same time. We then use it as a map of candidate positions.

The filters have exponential profiles and are adjusted so that the convolution with a constant values, such as an empty area of an image, gives zero as output. Each filter is equal to zero for $r = 3\alpha$ and $r = 6\alpha$ (which means that it weights as positive everything inside $r = 3\alpha$ – the typical size of an exponential object of scalelength 3α – and subtracts whatever is between $r = 3\alpha$ and $r = 6\alpha$). In this way, we obtain a scale selective filter: everything that is smaller or bigger than the filter scale size is severely dimmed.

The cleaned image is convolved with each filter and the output is a series of convolved images. Each of them improves the S/N of objects with scale sizes matching the filter scale. Using these convolved images we build a final output image whose value in each pixel is equal to the maximum value assumed in the stack of convolved images.[7] The main property of this final image is that objects corresponding to all the different sizes of filters are emphasized at the same time (Fig. 6).

The final image is used as a map for the positions of candidate galaxies; both detection and photometry are then performed on it.

[6] The theoretical trend of the stellar locus is also easily representable assuming a Gaussian radial profile with a width equal to the point spread function (PSF).

[7] The intensity on each convolved image is measured as multiples of the convolved image noise, so that the measure of intensities on different convolved images can be compared.

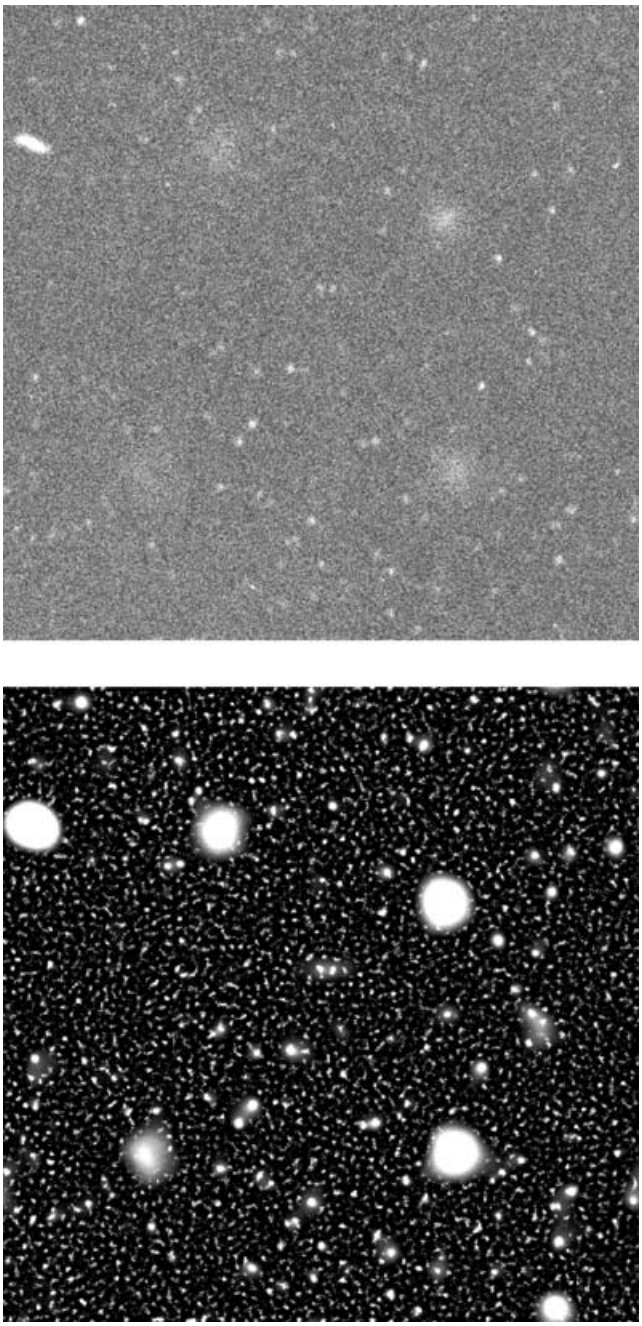

Figure 6. The top figure is a real image to which we added three artificial galaxies of scalelength (arcsec) and central surface brightness (flux per arcsec^2) as follows: (5, $1\sigma_{\rm sky}$), (4, $2\sigma_{\rm sky}$), (3, $3\sigma_{\rm sky}$). The two top-left detections are real galaxies in the image. The bottom figure is the final output of the algorithm. It is clear that the S/N ratio is improved and they are easily detectable.

It is a *significance image* (as the value of each pixel is expressed in multiples of noise of the convolved image corresponding to the best-matching filter) and the detection of the candidates is performed taking all peaks above a 3σ threshold (see Section 4.4). On a different array we save the filter scale on which each maximum for each pixel is found. That filter scale corresponds to the best-matching scale, and this is our estimate of the scalelength of the object.

From a computational point of view, once the filter scale sizes are decided, the set of filter arrays are built just once and then restored in the code at the convolution step. As a first application, we use filters with a radial symmetry, but the code also allows for the possibility of using an elliptical symmetry, which is optimized for edge on or intrinsically elongated objects.

The peak value on the output image also contains all the information we need for the photometry of the object, as shown in the following section.

4.4 Candidate classification: parameter estimation

Given the properties of the filters (see Section 4.3) it can be shown that when the scale size of the filter H matches the scale size of the galaxy h (which is the filter scale for which the value of the convolution is found to be maximum), the value of the convolution integral is

$$I = \int f_0 \mathrm{e}^{-r/h}\left(F_* \mathrm{e}^{-r/H}\right) 2\pi r \, \mathrm{d}r = \frac{F_*}{2}\pi f_0 h^2 \tag{4}$$

where $f_0\, \mathrm{e}^{-r/h}$ is the assumed exponential profile of the galaxy and $F_*\, \mathrm{e}^{-r/H}$ is just the positive part of the filter, as the object has zero flux on the negative part. Knowing the best-matching scale, which corresponds to our best estimation of the object scalelength, we can estimate the central original flux as

$$f_0 = \frac{I}{2\pi h_{\rm best}^2 F_*} \tag{5}$$

and calculate the central surface brightness.

In the ideal case of a Poissonian distribution for pixels in the image and assuming pixels to be uncorrelated, we can derive a simple relationship between the noise of the original image ($\sigma_{\rm i}$) and the noise in each convolved image ($\sigma_{\rm o}$). Within these assumptions, for a convolution with a simple $n \times n$ box filter, the noise reduction is

$$\sigma_{\rm o} = \frac{\sigma_{\rm i}}{\sqrt{n}}. \tag{6}$$

The relation still holds for the exponential filters and in general we can then write

$$\sigma_{\rm o} = k(H)\sigma_{\rm i} \tag{7}$$

where the coefficient k is different for each filter and is related to the filter scale size H.

Using equations (5) and (7) we can then show how the detection threshold on the final convolved image ($t = N_t\sigma_{\rm o}$) relates to a threshold in the minimum central surface brightness which is detected for each scalelength:

$$f_{0,\rm min} = \frac{t}{2\pi h^2 F_*} = \frac{N_t k(h)}{2\pi h^2 F_*}\sigma_i. \tag{8}$$

However, the assumption that pixels are uncorrelated is not completely true (because of the PSF) and these relationships need to be calibrated for our data. In order to calibrate them, we have used artificial galaxies added to real images. The results of these simulations are shown in the following section.

4.5 Artificial galaxy simulations

In order to test the efficiency of the method, we ran simulations using artificial galaxies added to real images. The use of artificial galaxies allows us to test the algorithm, exploring systematically the parameter space of scalelength (h) and central surface brightness (μ_0) and thus total magnitude. The added artificial galaxies have exponential profiles (as observations indicate that this is the best

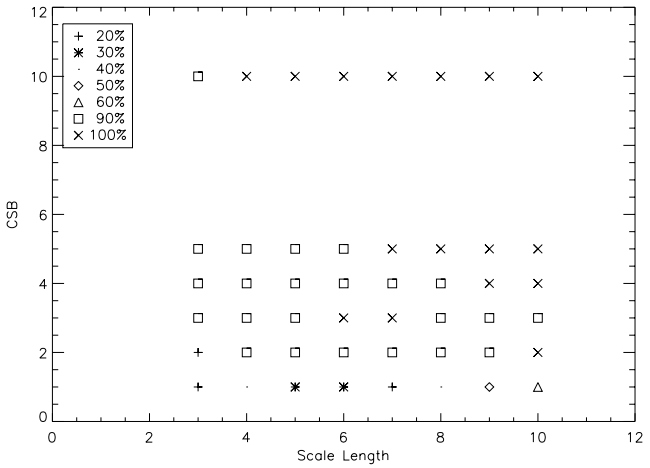

Figure 7. Detection efficiency plotted as a function of scalelength h and μ_0. The central surface brightness (μ_0) is measured as a multiple of the sky noise and in our images this corresponds to: $1\sigma \sim 26.1$, $2\sigma \sim 25.3$, $3\sigma \sim 24.9$, $4\sigma \sim 24.6$, $5\sigma \sim 24.3$, $10\sigma \sim 23.6$ mag arcsec^{-2}. As shown in the plot, different symbols refer to different efficiencies.

representation for dwarf and LSB galaxies profiles. See Davies et al. 1988), are convolved with a Gaussian that simulates the seeing and are added to the real data with their Poissonian noise. The use of these simulations allows us to determine the efficiency for detection and photometry of the objects.

In Fig. 7 we plot the efficiency of detection as a function of scalelength and central surface brightness of the artificial galaxies, where different symbols refer to different efficiencies. The efficiency is very high (90–100 per cent) over almost all of the simulated region. As expected, the efficiency drops for small and faint objects because of their low S/N. We now have an estimate of completeness and contamination of our detection method and we can correct for these effects. The objects that we can detect are just the objects we want to look for in Virgo. The faintest and smallest galaxies we are able to detect correspond to $M_B \sim -9.5$ and the brightest and biggest to $M_B \sim -14.5$.

Once detected, and knowing the best-matching filter scale, we can determine the central surface brightness (using equation 5) and thus the total magnitude of the objects. In Fig. 8 we show the difference between input and recovered values for the total magnitudes of the simulated galaxies. The efficiency in recovering the object's scalelength is strongly dependent on how big the gap is between the scale size of different filters. In order to obtain a good sampling of the scalelengths that we expect for dwarfs in Virgo, we decided to use the following 2, 3, 4, 5, 6, 7 and 9 arcsec filter scales. Although we used smaller filters the final minimum scale size for objects in our Virgo sample is 4 arcsec (see Section 3.1 for comments on this).

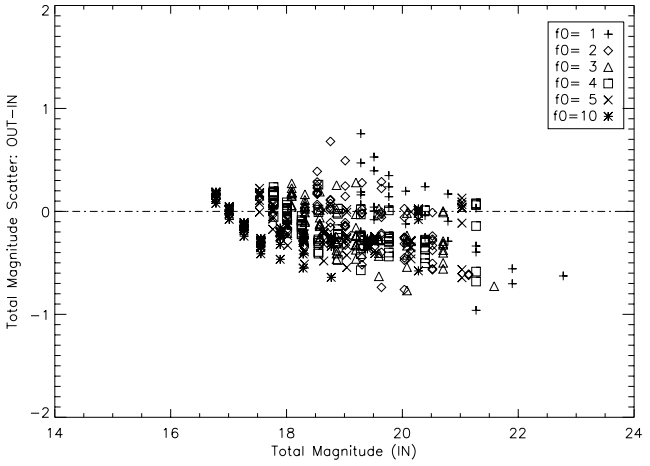

Figure 8. The measured magnitude minus input magnitude is plotted against input total magnitude. Different symbols refer to different values of μ_0. The biggest errors are for very faint objects.

Although we do have some scatter in the recovered scalelength and central surface brightnesses, the two compensate to give an estimation of the total magnitude with mean error of ± 0.5.

The standard way of measuring photometric parameters is by fitting to the radial surface brightness profile. The detection and fitting are two distinct operations. Using our method we maximize our detection efficiency by detecting the entire image, rather than just its poor S/N edge, and we also obtain the best-fitting parameters at the same time.

5 FIRST RESULTS: THE LF

5.1 The radial number density profile of the cluster

Clusters are very interesting regions to study in order to understand the role played by the environment on galaxy formation and evolution. They are also important because it might be expected that the cluster population surface density decreases with radius from the cluster centre and eventually merges into the field. This would imply that the properties of galaxies in the outskirts of the cluster must be linked to those of the field population.

The sample of galaxies that we have detected with our technique extends from the centre of the cluster (identified as M87) outward for 7°. Over the resulting area of $\sim$14 deg^2 we have identified 105 new extended dwarf LSB galaxies previously uncatalogued (see VCC; Impey et al. 1988; Trentham & Hodgkin 2002).

However, before discussing the implications on the LF, we need to demonstrate that we have a Virgo cluster sample rather than a sample contaminated by background (or foreground) objects.

Background contamination has been one of our main concerns. In Fig. 9 we have plotted the surface number density of our

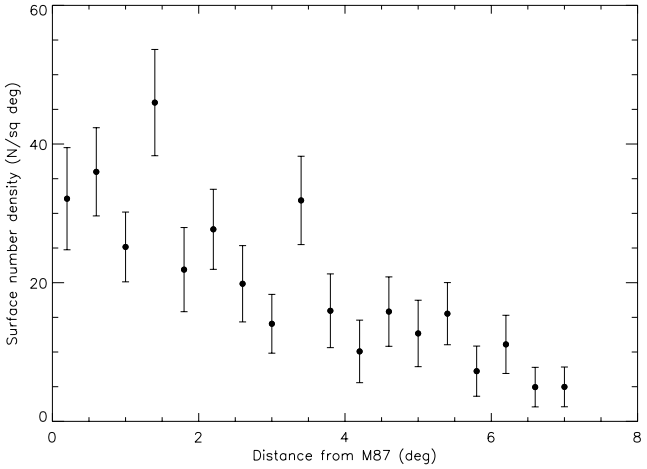

Figure 9. In this figure we plot the number density profile of the galaxies detected within our selection criteria ($h \geqslant 4$, $\mu_0 \geqslant 23$) versus distance from the cluster centre (identified as M87). As expected for a cluster member population, the density decreases when going further from the centre and eventually drops to almost zero approaching the cluster edge.

detections against cluster radius. This is the raw data – there are no corrections for contamination or completeness in this plot. As expected for a cluster member population, the density decreases when going further from the centre and eventually drops to an almost constant value close to zero, approaching the cluster edge. If our sample were highly contaminated by background galaxies, we would expect an almost flat distribution of galaxies, not one dependent on distance from the centre of the cluster.

An exponential plus a constant (background) fit to the distribution gives a scalelength of $2.2^\circ \pm 0.2^\circ$ (at the distance of the Virgo cluster this corresponds to 0.7 Mpc) and a background galaxy density of 5 ± 1 galaxies per deg^2. This is consistent within the errors with the value of four galaxies per deg^2 found for the background in the offset fields described in Section 3.2 and can thus be considered as the non-member contamination in our sample. In summary, although there might still be some contamination by background galaxies, we have demonstrated it is minimal (see our numerical simulations, the offset field number counts and Fig. 9).

This radial distribution can be compared with that of the bright galaxies. We have defined a dwarf-to-giant ratio (DGR) which we will use in subsequent papers for comparison with different environments. This is the ratio of dwarf galaxies, defined as those with $-14 \leqslant M_B \leqslant -10$, to giant galaxies with $M_B \leqslant -19$. We use this quantity because in some environments there are too few galaxies to construct a LF.

In Fig. 10 we show this ratio as a function of distance from M87. Interestingly, this ratio remains rather flat with a median value of $\sim$20: the dwarf and giant numbers decline with clustercentric distance with the same scalelength, resulting in a constant DGR.

Sabatini et al. (2002) have shown evidence that the DGR is about 4 for the field population. This is just about the number that would be obtained with our selection criteria if observing the Milky Way from the distance of the Virgo cluster. Out of the group of galaxies that Mateo (1998) assigns to the Milky Way just the dwarfs Sextans Fornax and Sagittarius would meet our selection criteria. Again this would give a value for the DGR of 3, lower than in Virgo. As most dwarf galaxies in clusters are probably not bound to individual giant galaxies we can also do the same test for all the dwarfs in the Local Group, in order to compare it with the Virgo cluster. Again we obtain a DGR of 4.

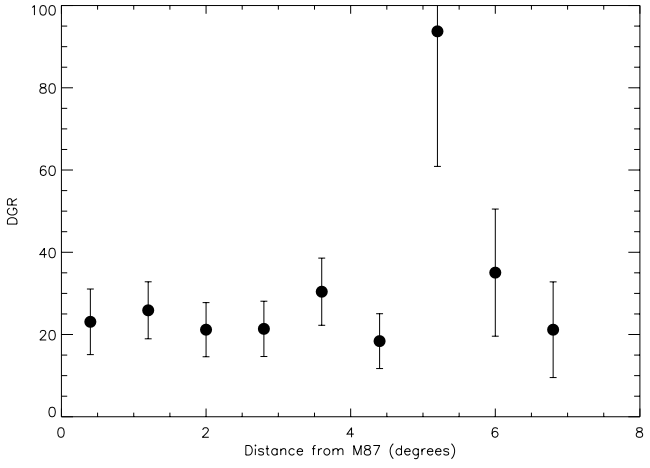

Figure 10. DGR as a function of distance from M87. Here we define the dwarf galaxies with $-14 \leqslant M_B \leqslant -10$ and the giant galaxies with $M_B \leqslant -19$. The peak at $\sim 5^\circ$ is mainly due to a dip in the distribution of giants and not to an excess of dwarfs.

Also, interestingly, the Virgo cluster DGR does not appear to smoothly blend into the field; if it did we would expect the DGR to gradually decrease to the value in the field. Note also that we must be close to the 'edge' of the cluster because the galaxy counts are about the same as those in our offset fields. Thus, the Virgo cluster environment seems to be very different to that of the field even in its most outer regions.

5.2 The faint-end slope of the LF

In this paper we are primarily interested in the number of dwarf galaxies in the cluster. When sufficient galaxies are available this is found by fitting to the faint end of the LF. Our method enables us to detect galaxies with the following range of absolute magnitudes: $M_B = -10$ ($h_{\rm min} = 4$ arcsec, $\mu_0^{\rm min} = 26\ B\mu$) to $M_B = -15$ ($\mu_0^{\rm max} = 23\ B$ mag arcsec^{-2}, $h_{\rm max} = 9$ arcsec).

An important check is to compare our derived magnitudes with galaxies common to previous catalogues of the Virgo cluster. We have 143 galaxies in our sample that are listed in Trentham & Hodgkin (2002) and we show a plot of our measured apparent magnitudes against the measurements of Trentham et al. in Fig. 11. A linear fit to this plot results in a slope of 1.02 and a constant value of -0.22. Our magnitudes tend to be slightly brighter than those of Trentham et al., but the difference lies within the errors we expect in our measurements (see Fig. 8). Galaxies listed in Trentham & Hodgkin (2002) that are not in our sample have been checked and they are either too bright to fall within our surface brightness range or they lie in masked regions of the images (in our calculations we take into account the area lost due to the removal of stars).

Our derived LF is shown in Fig. 12. We show the raw data and the corrected data. The number of objects detected in each bin of h and μ_0 has been corrected for:

(i) background contamination (as obtained from our numerical simulations of a cone of the universe);

(ii) incompleteness (as estimated by the detection efficiency of the algorithm with artificial galaxies).

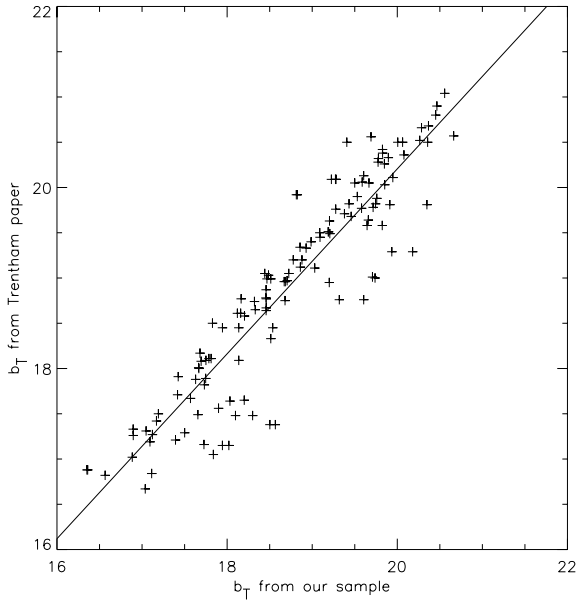

Figure 11. Comparison between apparent magnitudes as measured with our method (x-axis) and those in Trentham & Hodgkin (2002). A linear fit to the data gives a slope of 1.02 and a constant of -0.22.

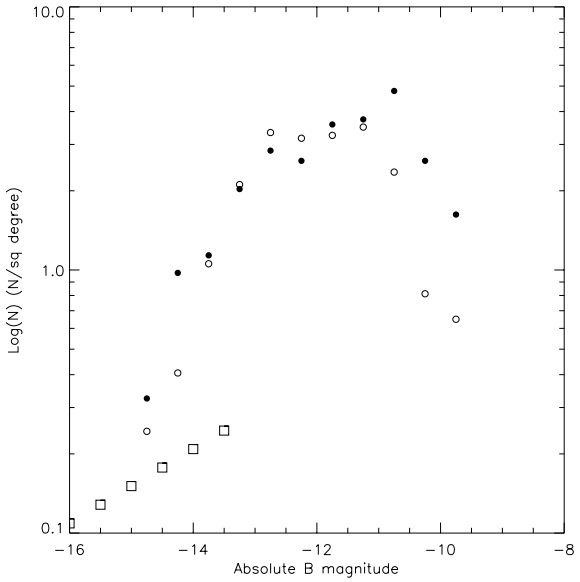

Figure 12. In this figure we plot the faint end of the LF. Open circles are counts for the raw data, while solid circles are corrected for detection efficiency and background contamination. Squares are points from the VCC LF with slope $\alpha = -1.35$, renormalized for our survey area.

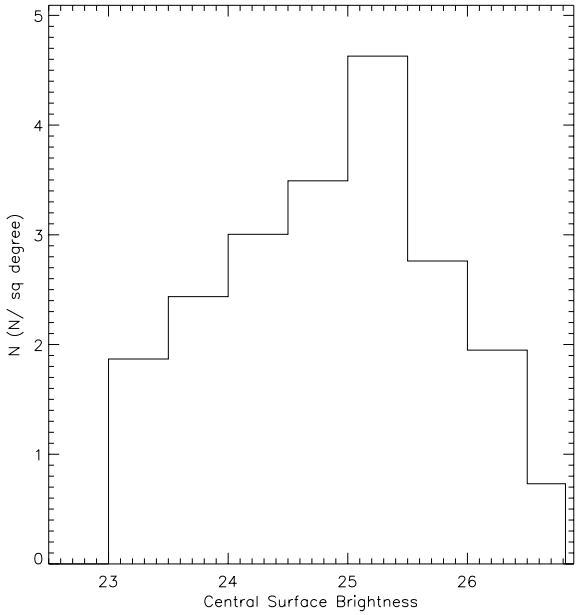

Figure 13. Histogram of central surface brightness distribution for our detections.

The corrections make little difference to the numbers detected in each bin, for magnitudes brighter than -11. Assuming that the drop-off in numbers beyond $M_B = -10.5$ is due to incompleteness, we have fitted the LF in the magnitude range -14.5 to -10.5. This gives a value for the faint-end slope of -1.7 ± 0.2 for the raw counts and -1.6 ± 0.1 for the counts corrected for incompleteness.

It is difficult to combine galaxy counts from samples selected in different ways. For example, Kambas et al. (2000) show how the selection of three different samples of galaxies leads to a disjoint surface brightness distribution because in each case the selection criteria preferentially picks galaxies of a given surface brightness. The surface brightness distribution of this sample (Fig. 13) is also peaked.

Even so, in Fig. 12 we have also shown, for comparison, the number counts for the VCC.[8] Including the VCC data and fitting the faint-end slope between -16 and -10.5, we obtain a value of -1.8 for α.[9] The values that we obtain are in agreement with a steepening of the LF when including in the sample the contribution from faint and LSB galaxies. The original VCC value of -1.35 (Sandage et al. 1985b) had already been brought into question by Binggeli, Sandage & Tammann (1988) who suggested a steepening to -1.7 when including a possible dwarf population that had escaped detection. The final slope we obtain is not as steep as that obtained by Phillipps et al. (1998a) using the background field subtraction method. However, in order to compare our results with those of Phillipps et al. we should consider our raw data counts (as they did not make any correction for incompleteness) that result in a slope of -1.7 ± 0.2. Neglecting the last point in their LF, which might be highly background contaminated (S. Phillipps, private communication), their slope is $\sim -1.9 \pm 0.15$. This then is consistent with our result.

We can also calculate a separate LF for the inner (dashed-dotted line) and outer (solid line) regions of the cluster (see Fig. 14). We have chosen these regions because they correspond roughly to that part of the cluster that is within the virial radius and that which is outside it. Galaxies within the virial radius should have been much

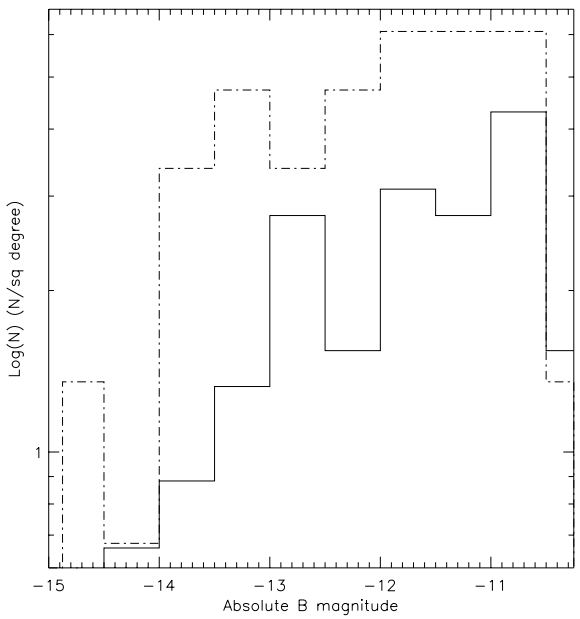

Figure 14. In this figure we plot the faint-end part of the LF separating the cluster into an inner (distance from M87 $\leqslant 0.8^\circ$) and outer (distance from M87 $\geqslant 1.6^\circ$) region. The dashed-dotted line refers to the inner region, while the solid line refers to the outer region. Although the numbers give poor statistics, a K–S test shows that the two distributions are different with a 90 per cent probability. A fit to the same range of magnitudes as for the total LF gives a steeper value for the faint-end slope of the LF in the outer region compared with the inner region (-1.8 ± 0.2 and -1.4 ± 0.2).

[8] These can also be used to compare our data with the number counts obtained in Trentham & Hodgkin (2002), as their findings fit very well with the LF of the VCC (see their figure 5).

[9] We cannot write an error on this value because we do not have a completeness function for the VCC catalogue.

more affected by interactions with other cluster galaxies than those in the dynamically unrelaxed outer regions (Bohringer 1995). A fit to the same range of magnitudes as for the total LF results in a steeper value for the faint-end slope in the outer region compared with the inner (-1.8 ± 0.2 and -1.4 ± 0.2). A Kolmogorov–Smirnov (K–S) test shows that the two distributions are different with a 90 per cent probability. If confirmed by larger statistics, this result is consistent with the idea that the faintest galaxies are more abundant in the outer regions of clusters, while in the denser inner regions they have partly been accreted by larger galaxies or have dimmed or even been disrupted by tidal interactions.

5.3 Total luminosity and mass

The total light (corrected for the area of the cluster sampled compared to the VCC) due to the population of dwarf LSB galaxies of our sample is

$$L_{\rm Dwarf} = 4 \times 10^9 \, {\rm L}_\odot \tag{9}$$

which is just 1/50 of that due to VCC galaxies. So this population of galaxies contributes only a small fraction of the light contributed by the bright galaxies.

A surface brightness level of about $28\,B$ mag arcsec^{-2} has recently been predicted for intracluster light from stars associated with intracluster planetary nebulae (Arnaboldi et al. 2002). The average integrated surface brightness from the galaxies we detected is $\mu_{\rm tot} \approx 32$ mag arcsec^{-2} in the inner region of the cluster (within 0.8° from M87). This is far too faint to have been previously detectable as a surface brightness enhancement. This, combined with the planetary nebulae data, may indicate that there are more even lower surface brightness structures to be discovered between the galaxies.

Despite the small contribution to the light, dwarf galaxies may contribute a larger fraction to the mass. Recently very large mass-to-light ratios have been found for Local Group galaxies (Mateo 1998; Kleyna et al. 2002). Assuming a mass-to-light relation as in Davies et al. 2003

$$\frac{M}{L} = 10^{3.5} L^{-0.25}, \tag{10}$$

the total mass due to the dwarf LSB population over the strip effective area of 13. 14 deg^2 is

$$M_{\rm Dwarf} = 1.9 \times 10^{11} \, {\rm M}_\odot. \tag{11}$$

Rescaled to the total area of the cluster, this is 1/10 of the total mass from the VCC galaxies. Given that other LSB material associated with intracluster stars exists, it is possible that there is as much mass in the LSB component of the Virgo cluster as there is in the brighter galaxies.

6 CONCLUSIONS

Observations of the relative numbers of dwarf galaxies in different environments present a strong challenge to galaxy-formation models that predict large numbers of dwarf galaxies in all environments. They also present a challenge to those models that predict global suppression of dwarf galaxy formation. The Virgo cluster is a very different environment from that of the Local Group and from that of the general field. It has a very large number of dwarf galaxies compared to the giant galaxy population.

In this paper we have described a new automated technique for finding LSB galaxies on wide-field CCD data. We have carried out simulations to ensure that our detection method and selection criteria enable us to preferentially select cluster galaxies, rather than those in the background. From the decrease in surface number density with clustercentric distance we believe that we have achieved this goal.

Over the resulting area of $\sim$14 deg^2 that we analysed, we have identified 105 new extended dwarf LSB galaxies previously uncatalogued (see VCC; Impey et al. 1988; Trentham & Hodgkin 2002). The resulting LF is considerably steeper than that inferred from an extrapolation of the data in the VCC. The cluster LF appears to be steeper in the outer parts of the cluster than in the inner part, although the DGR remains almost constant. Although these galaxies contribute only a small fraction of the luminosity of the cluster they may contribute significantly to the galactic mass of the cluster, given recently measured large mass-to-light for Local Group dSph galaxies.

REFERENCES

Armandroff T. E., Davies J. E., Jacoby G. H., 1998, AJ, 116, 2287
Arnaboldi M. et al., 2002, AJ, 123, 760
Bernstein G. M., Nichol R. C., Tyson J. A., Ulmer M. P., Wittman D., 1995, AJ, 110, 1570
Bertin E., Arnouts S., 1996, A&AS, 117, 393
Binggeli B., Sandage A., Tarenghi M., 1984, AJ, 89, 64
Binggeli B., Sandage A., Tammann G. A., 1985, AJ, 90, 1681
Binggeli B., Tammann G. A., Sandage A., 1987, AJ, 94, 251
Binggeli B., Sandage A., Tammann G. A., 1988, ARA&A, 26, 509
Blanton M. R. et al., 2001, AJ, 121, 2538
Bohringer H., 1995, Ann. New York Acad. Sci., 759, 67
Bothun G. D., Impey C. D., Malin D. F., 1991, ApJ, 376, 404
Bullock J. S., Kravtsov A. V., Weinberg D. H., 2000, ApJ, 539, 517
Conselice C. J., Gallagher J. S., Wyse R. F. G., 2001, ApJ, 559, 791
Cross N. et al., 2001, MNRAS, 324, 825
Davies J., Phillipps S., Cawson M., Disney M., Kibblewhite E., 1988, MNRAS, 232, 239
Davies J., Linder S., Roberts S., Sabatini S., Smith R., Evans R., 2003, MNRAS, submitted
Dekel A., Silk J., 1986, ApJ, 303, 39
Driver S., 1999, AJ, 526, L69
Efstathiou G., 1992, MNRAS, 256, 43 P
Flint K., Metevier A. J., Bolte M., De Oliveira C. M., 2001, ApJS, 134, 53
Fouque P., Solanes J. M., Sanchis T., Balkowski C., 2001, A&A, 375, 770
Gavazzi G., Bonfanti C., Sanvito G., Boselli A., Scodeggio M., 2002, ApJ, 576, 135
Impey C., Bothun G., Malin D., 1988, ApJ, 330, 634
Kambas A., Davies J., Smith R., Bianchi S., Haynes J., 2000, AJ, 120, 1316
Kleyna J., Wilkinson M. I., Evans N. W., Gilmore G., Frayn C., 2002, MNRAS, 330, 792
Lahav O. et al., (the 2dFGRS team), 2002, 5th RESCEU Symp. Universal Academy Press, Tokyo
Liske J., Lemon D. J., Driver S. P., Cross N. J. G., Couch W. J., 2003, MNRAS, submitted (astro-ph/0207555)
Madgwick D. et al., 2002, MNRAS, 333, 133M
Mateo M. L., 1998, ARA&A, 36, 435M
Moore B., Lake G., Quinn T., Stadel J., 1999, MNRAS, 304, 465M
Morshidi-Esslinger Z., 1997, PhD thesis, Univ. Cardiff
Phillipps S., Parker Q., Scwhartzenberg J., Jones J. B., 1998a, ApJ, 493, L59
Phillipps S., Driver S. P., Couch W. J., Smith R. M., 1998b, ApJ, 498, L119
Russell J. S., Lucey J. R., Hudson M. J., Schlegel D. J., Davies R. L., 2000, MNRAS, 313, 469
Sabatini S., Scaramella R., Testa V., Andreon S., Longo G., Djorgovsky G., De Carvalho R. R., 1999, Mem. S. A. It, 71, 1091
Sabatini S., Roberts S., Davies J., 2002, in Lobo C., Serote Roos M., Biviano A., eds, JENAM Workshop, Galaxy Evolution in Groups and Chisters. Kluwer, Porto, in press
Sandage A., Binggeli B., 1984, AJ, 89, 919S

Sandage A., Binggeli B., Tammann G., 1985a, AJ, 90, 395
Sandage A., Binggeli B., Tammann G., 1985b, AJ, 90, 1759
Shapley H., Ames A., 1932, Ann. Harvard College Observatory. Cambridge. MA
Shibata R., Matsushita K., Yamasaki N. Y., Ohashi T., Ishida M., Kikuchi K., Böhringer H., Matsumoto H., 2001, ApJ, 549, 228
Tikhonov N. A., Galazutdinova O. A., Drozdovskii I. O., 2000, Ap, 43, 367
Trentham N., Tully B., Vereijen M., 2001, MNRAS, 325, 385
Trentham N., Hodgkin S., 2002, MNRAS, 333, 423
Trentham N., Tully R. B., 2002, MNRAS, 335, 712
Tuffs R. et al., 2002, ApJS, 139, 37
Tully R. B., Somerville R. S., Trentham N., Verheijen M. A. W., 2002, ApJ, 569, 573
Valotto C. A., Moore B., Lambas D. G., 2001, ApJ, 546, 157
Van Driel W., Ragaigne D., Boselli A., Donas J., Gavazzi G., 2000, A&AS, 144, 463

This paper has been typeset from a TEX/LATEX file prepared by the author.